SigmoidOxy: A light-weight mobile perfusion tool for diabetic foot management

Alexander Gherardi
University at Buffalo
Buffalo, New York, USA
ajgherar@buffalo.edu

Ahmet Y. Demirbas
University at Buffalo
Buffalo, New York, USA
ahmetdem@buffalo.edu

Wenyao Xu
University at Buffalo
Buffalo, New York, USA
wenyaoxu@buffalo.edu

Abstract

Diabetic foot ulcers (DFUs) represent a significant global health challenge for the elderly with high mortality rates and complications. While imaging technologies like NIRS and hyperspectral imaging have improved wound assessment in clinical settings, their cost, and large size limit their use in the home and primary care. On the other hand, existing mobile solutions only capture secondary bio-markers like color and wound size. This paper introduces SigmoidOxy (or σ(Oxy)), a novel smartphone-based perfusion tool for DFU management. SigmoidOxy extracts oxygenation information from standard RGB images captured by smartphone cameras by applying hyperspectral reconstruction models to infer oxygenation. We evaluate SigmoidOxy's performance using the SPECTRALPACA dataset [2] finding an Average Persons R of 0.72 and Average Mean Absolute Error of 0.239 when comparing sigmoid oxygenation signals and analyze its sensitivity to ischemia in the DFUC2021 dataset [17].

Keywords

Spectral Reconstruction, Mobile Health, Diabetic Foot Ulcers

ACM Reference Format:

Alexander Gherardi, Ahmet Y. Demirbas, and Wenyao Xu. 2024. SigmoidOxy: A light-weight mobile perfusion tool for diabetic foot management. In *The 30th Annual International Conference on Mobile Computing and Networking (ACM MobiCom '24), November 18–22, 2024, Washington D.C., DC, USA*. ACM, New York, NY, USA, 7 pages. https://doi.org/10.1145/3636534.3698119

ACM MobiCom '24, November 18–22, 2024, Washington D.C., DC, USA

ACM ISBN 979-8-4007-0489-5/24/11
https://doi.org/10.1145/3636534.3698119

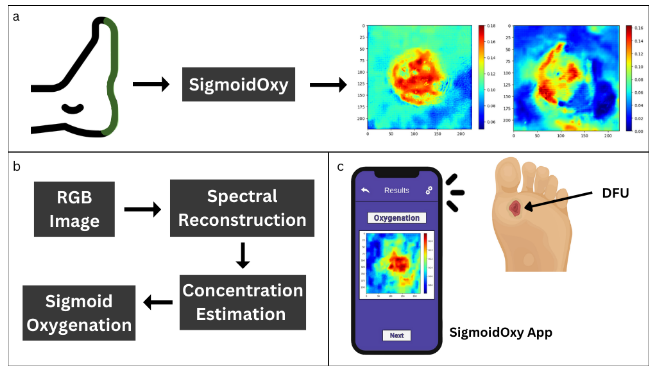

Figure 1: SigmoidOxy – A smartphone-based system for DFU management: (a) SigmoidOxy processes an RGB image of a foot to produce an oxygenation map; (b) A schematic diagram showing the processing pipeline from RGB image input through spectral construction and concentration estimation to produce SigmoidOxy output; (c) SigmoidOxy UI visualizing oxygenation at a DFU site.

1 Introduction

Chronic wounds, particularly diabetic foot ulcers (DFU), affect millions of individuals worldwide. Five-year mortality rates for DFU exceed 25% in individuals who experience complications [1]. Early detection, accurate assessment, and regular monitoring of these wounds are vital. However, for the elderly population, especially those with mobility issues, which are common in individuals with chronic wounds, getting to a clinic can be impractical, and home visits from clinicians can be prohibitively expensive, leading to delayed discovery of infections and complications in the healing process [13].

Near Infrared Spectroscopy (NIRS) [12] and hyperspectral imaging [11] in recent years have become the gold standard for capturing and imaging physiological biomarkers that give specialists insight into the condition of a wound on devices for hospital and clinical use. However, even though these cameras are highly promising for the clinical setting, they are still bulky and extremely expensive, making them completely inapplicable for home care and primary care settings. On the other hand, researchers have been developing mobile solutions for foot ulcer monitoring that, instead of working to capture oxygenation and perfusion, examine secondary characteristics of the wound, such as its color and diameter, which can be ascertained from a simple RGB photograph. However, since these are secondary characteristics, they do not provide the same level of insight into wound health as oxygenation would be able to.

Outside of diabetic foot ulcers, researchers have applied Wiener Filters to reconstruct full hyperspectral images from RGB images taken on smartphones [6, 7]. However, given that this methodology for performing hyperspectral reconstruction just boils down to linear matrix multiplication, ultimately, it is unable to, by nature, introduce any information not already present in a single RGB pixel in the input image. More importantly, outside of mobile health, hyperspectral reconstruction using deep learning is soon approaching the point where it looks like it will be possible to perform reconstruction under arbitrary lighting and with any smartphone without requiring retraining [9]. And previously, dictionary learning [5] has been used to simultaneously estimate lighting conditions and material reflectance directly with larger datasets now available that include reflectance and RGB image pairs. We believe that we will soon see deep learning applied to this task. With this in mind, we propose a new methodology based on modern image-to-image spectral reconstruction as described in recent literature [8] pertaining to spectral reconstruction and demonstrate its use here while addressing any implementation challenges we come across.

In this paper, we present SigmoidOxy, a novel smartphone-based perfusion tool that extracts oxygenation information directly from ordinary RGB images captured by smartphone cameras and leverages this as a biomarker for wound perfusion in actual captured DFU images.

Our major contributions are as follows:

(1) A smartphone-based perfusion tool for the assessment of chronic wounds.
(2) A demonstration of modern hyperspectral reconstruction models being applied to determine oxygenation.
(3) A new biomarker for oxygenation that is robust to outliers and pairs well with our system.
(4) A detailed evaluation of the performance of our approach on the SPECTRALPACA dataset [2] and a preliminary analysis of its sensitivity to ischemia in the DFUC2021 dataset [17].
(5) A user-friendly smartphone application designed for elderly users and those with limited technical proficiency.

2 System Principle and Design

In this section, we outline and detail the architecture and rationale behind each stage of our system which leverages a pre-trained spectral reconstruction model and classical reflection spectroscopy techniques to extract oxygenation information from ordinary RGB images and videos.

2.1 Background

Human skin is highly complex and contains many unique chromophores, some of which may only be present in individuals of a certain ethnic background (e.g., skin tone) or skin condition (e.g., smoking introduces a higher concentration of carboxyhemoglobin). In addition to this skin is multi-layer [16], and the resulting absorption/reflectance spectra integrates contributions from each layer differently depending on its thickness and depth. The situation is further complicated in cases where wounds are present, which may contain additional chromophores depending on their condition and different layer compositions. All this ignores any non-linear scattering effects as well.

2.2 Spectral Reconstruction

Due to the inherent variability of skin (especially wounded skin) and skew in the distribution of key skin parameters such as skin tone mixed with the difficulties of collecting data from populations with chronic wounds (who struggle with mobility issues and pain) and the expense of collecting data with hyperspectral cameras. We do not believe that constructing reconstruction models by training on datasets involving only images of skin is the best way here to produce results that exhibit low bias in this case.

For this and the reasons outlined in the introduction pertaining to the direction the field is moving toward we apply MST++ [3], a deep learning spectral reconstruction model pre-trained on a wide set of images taken with a hyperspectral camera under various scenarios (such as of plants and environments, indoors and outdoors) such that it can reconstruct a hyperspectral image generally.

2.3 Concentration Estimation

Once the skin spectra have been recovered using the model. It's straightforward and analytic to go from spectra to the chromophores concentrations [4] if you already have the chromophore spectral intrinsics [14, 15] and assume there are no non-linear scattering effects or anything of the like. The Beer-Lambert law relates reflected/transmitted $T(\lambda)$ and absorbed spectra $A(\lambda)$ to material concentrations in a sample.

$$A(\lambda) = -\ln T(\lambda) = \varepsilon(\lambda) \cdot c \cdot l. \tag{1}$$

As MST++ and other spectral reconstruction models do not include the original/physically accurate scale for their transmittance/reflectance spectra as even with a true hyperspectral camera this scale comes from calibration white and dark calibration targets which are not available in this case. This lack of scale causes numerical issues with the sharp asymptote that ln has at 0. We note, however, that in the range $[\frac{1}{20}, \quad 1]$, there is no strong non-linear behavior, and a linear approximation works well. So, we apply the approximation to the Beer-Lambert law and use that for our further analysis, since by definition reflectance values are bounded between 0 and 1, and in only the darkest materials do they fall below $\frac{1}{20}$.

$$A(\lambda) \approx -T(\lambda) \approx \varepsilon(\lambda) \cdot c \cdot l \tag{2}$$

From here, we assume that skin only contains the 3 materials we are concerned with hemoglobin, oxyhemoglobin, and melanin (specifically eumelanin). Then using the molar extinction coefficient for each of these materials ($\epsilon_{\mathsf{Hb}}, \epsilon_{\mathsf{Hb02}}, \epsilon_{\mathsf{M}}$) and the previously outlined physical law. Taking the optical path-length l=1 as it would cancel out or become unimportant later anyway when we determine the oxygenation and defining $p = -T$. The spectral pixel can then be related to the material concentrations as follows.

$$\begin{aligned} p(i,j,\lambda) =& \epsilon_{\mathsf{Hb}}(\lambda) \cdot c_{\mathsf{Hb}}(i,j) + \epsilon_{\mathsf{Hb02}}(\lambda) \cdot c_{\mathsf{Hb02}}(i,j) \\ &+ \epsilon_{\mathsf{M}}(\lambda) \cdot c_{\mathsf{M}}(i,j) \end{aligned} \tag{3}$$

Enumerating this equation for the 31 wavelengths (λ) outputted by the spectral reconstruction such that there is now a system of 31 linear equations, then representing the system as a matrix equation with $\mathbf{E} = [\boldsymbol{\epsilon}_{\mathsf{Hb}}, \boldsymbol{\epsilon}_{\mathsf{Hb02}}, \boldsymbol{\epsilon}_{\mathsf{M}}]$, $\mathbf{c} = [c_{\mathsf{Hb}}, c_{\mathsf{Hb02}}, c_{\mathsf{M}}]$ and we can obtain

$$\mathbf{p} = \mathbf{Ec}. \tag{4}$$

For each pixel (i, j), Which can be solved for the concentrations vector **c** using linear least squares.

$$\mathbf{c} = \left(\mathbf{E}^T\mathbf{E}\right)^{-1}\mathbf{E}^T\mathbf{p}. \tag{5}$$

2.4 Sigmoid Oxygenation

Once the concentration vector is obtained, the oxygenation can be estimated. There are a few different ways to define tissue oxygenation. It is most common to define tissue oxygenation saturation as the fraction of oxygenated hemoglobin to all the hemoglobin present in the tissue. This, however, does not work here in the same way as even in the case of ground truth spectral data from spectral cameras, as we found that it is common for one of the concentrations to be negative. Therefore, in order to have a quantity that varies as one would expect with the actual tissue oxygenation, we must apply a different feature.

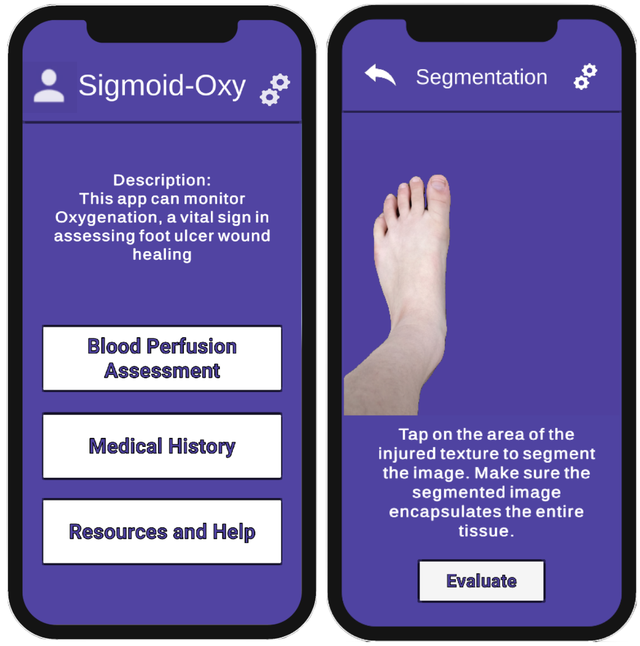

Figure 2: Main Menu and Results User Interface.

$$\sigma(O_2) = 1 - \sigma\left(\left|\frac{\mathsf{HbO_2}}{\mathsf{Hb}}\right|\right). \tag{6}$$

This feature, herein referred to as sigmoid oxygenation, has a simple rationale. Since the non-transformed absolute oxygenation feature $\left|\frac{\mathsf{Hb02}}{\mathsf{Hb}}\right|$ seems to increase when the actual tissue oxygenation is made to decrease, we must invert it. To invert this quantity, we first apply the sigmoid function to constrain the quantity to the range $[0, 1]$, after which we apply the $1 - x$ transformation to perform the inversion.

3 Application Development and Integration

3.1 User Interface Design

We implemented the Sigmoid-Oxy system as a smartphone app with an intuitive user interface (UI) to facilitate easy wound monitoring and assessment for patients. The app leverages the smartphone's camera and outlined algorithms to perform hyperspectral reconstruction and analysis of foot ulcers. The UI is structured to guide users through the assessment process, provide clear results, and maintain a record of historical data. To improve the user experience (UX) for the elderly and those with limited technical proficiency, we prioritize simplicity, accessibility, and guided workflows in our smartphone UI design. The UI is tailored towards the elderly, featuring large fonts, buttons, and a lot of visual feedback and animations. Users are walked through capturing and segmenting images and then interpreting results from the system (see Figure 2). Based on some simple analysis, the

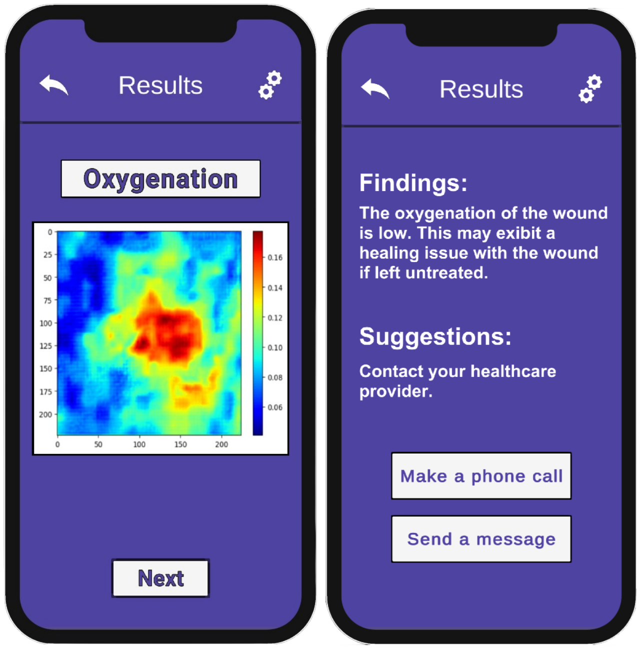

Figure 3: Segmentation and Diagnosis User Interface.

app provides a preliminary diagnosis and suggestions for wound care (see Figure 3). The app offers immediate guidance to users while emphasizing the importance of professional medical advice.

3.2 Implementation

We use the Segment Anything Model (SAM) [10] for the segmentation of photos of the foot to provide accurate wound boundary detection. The segmentation process is interactive; it allows the users to refine the selection if needed. We offload the heavy image processing required for our SigmoidOxy system to the cloud. Images taken with the smartphone are uploaded to a cloud serivce where the whole pipiline is ran, upon which the processed images are downloaded back to the smartphone for presentation to the user, allowing for the use of these capabilities on resource-constrained smartphones.

4 Evaluation

4.1 Oxygenation

To validate our system, we evaluated the quality of the generated sigmoid oxygenation signals and images against those produced by a true hyperspectral camera. To do so, we leverage the SPECTRALPACA dataset consisting of hyperspectral videos taken while a cuff was used to apply pressure to the arm of participants. Pressure was applied in increments with a release of pressure between each increment to allow tissue oxygenation to return to a nominal value. The appropriate regimen of preprocessing steps were applied to the raw hyperspectral images. First, each hyperspectral channel was spatially/spectrally calibrated using images taken of a white and dark target provided in the dataset. Then, using the channel's quantum sensitivity matrix, the channels were transformed into a 31-band spectral image with evenly spaced bands from 460-640nm. Following that a corresponding RGB

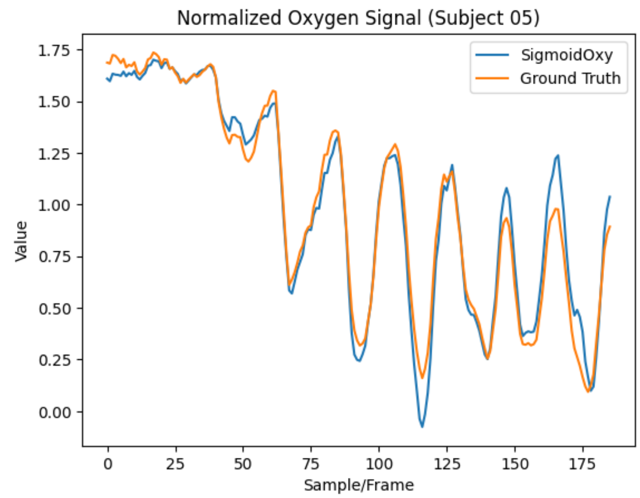

Figure 4: Processed and Normalized Sigmoid Oxygenation Signal between ground truth spectra and reconstructed spectra for subject 05.

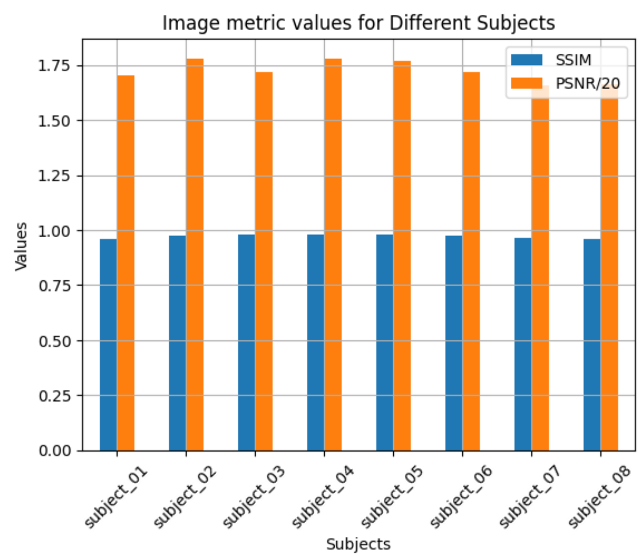

Figure 5: Image metric comparisons between ground truth spectra and reconstructed spectra for the first processed sigmoid oxygenation image in each subject video.

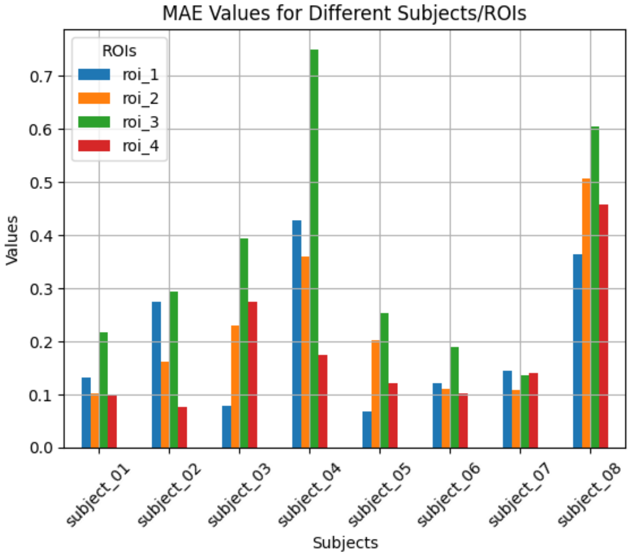

Figure 6: Mean Absolute Error metrics between ground truth spectra and reconstructed spectra for the processed and normalized sigmoid oxygenation signal in each subject region of interest.

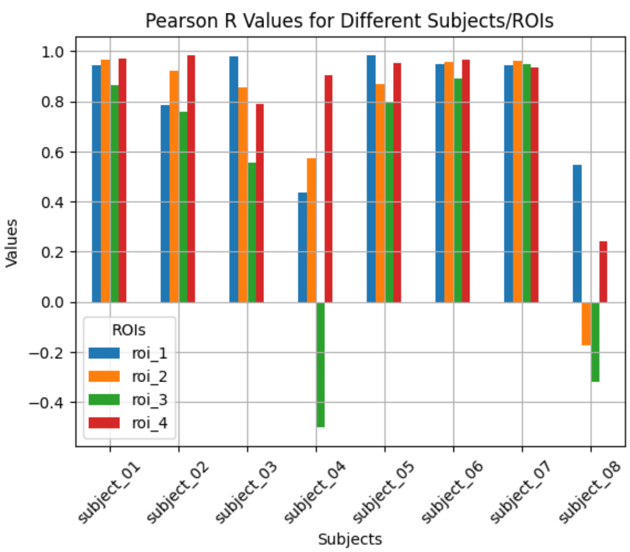

Figure 7: Pearson R metrics between ground truth spectra and reconstructed spectra for the processed and normalized sigmoid oxygenation signal in each subject region of interest.

image was generated using the quantum sensitivity matrix for a Samsung Galaxy smartphone rescaled to fit within 460-640nm.

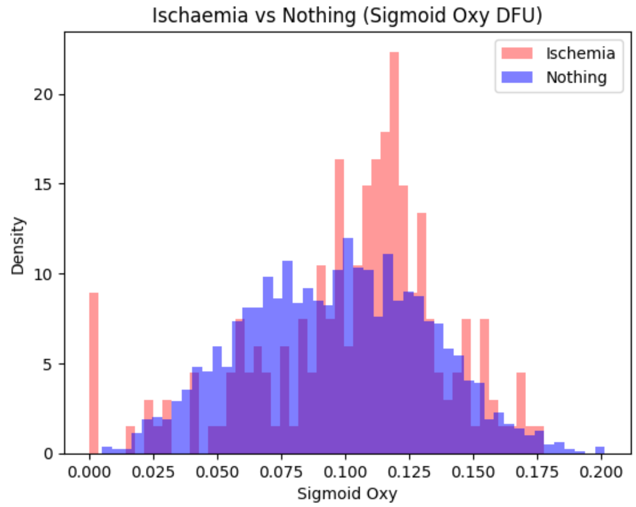

Figure 8: Distribution of Sigmoid Oxygenation values for Ischemia Foot Ulcers versus Normal Foot Ulcers.

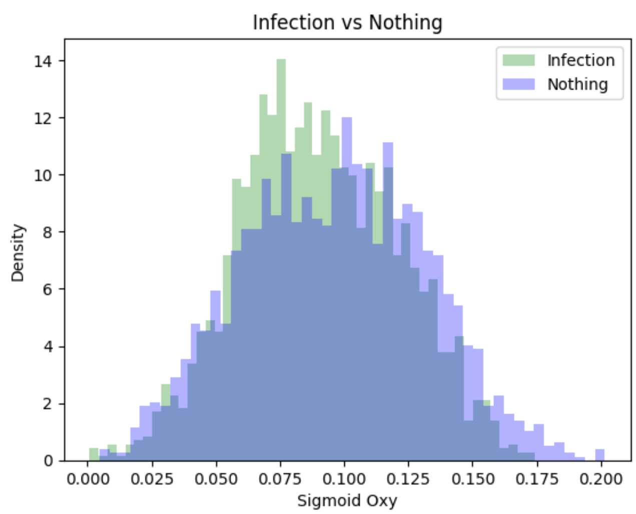

Figure 9: Distribution plot of Sigmoid Oxygenation values for Infection Foot Ulcers versus Normal Foot Ulcers.

Following that in order to adapt MST++ to work for RGB images generated with spectral information in the 460-640nm range (the original pretrained model is for 400-700nm RGB image) we retrained the model using its original dataset for 460-640nm generated RGB images. The rest of the system was left unmodified, and the following comparisons are between the sigmoid oxygenations that result from applying the rest of the system to the ground-truth hyperspectral data and the hyperspectral images that are outputted from MST++.

The agreement was tested in two different manners. First, the sigmoid oxygenation videos were downsampled temporally 90x. Then, the regions of interest (there are four) that were provided with the dataset were extracted framewise to form a patch sequence/signal. A patchwise mean was taken to form a 1D sigmoid oxygenation signal for each region of interest (ROI) and Subject combination. Mean absolute error and Pearson's R were used to compare the resulting signals, which were both normalized beforehand by subtracting the mean, dividing by twice the standard deviation, and adding one to produce a signal that ranges between $[0, 2]$. Figure 4 illustrates one such normalized pair of signals for an ROI on subject 5. The MAE values are plotted in Figure 6, and the Pearson's R values are shown in Figure 7. To test the image agreement, the first processed image from each subject's video was taken and then compared using PSNR and SSIM metrics after a large ROI was selected to ensure that the background (which was segmented) had minimal influence on the metric values, the metric values are shown in Figure 5.

4.2 DFU Evaluation

We then evaluated the performance of our system for distinguishing the presence of ischemia in actual images of diabetic foot ulcers provided by the DFUC2021 dataset [17]. The DFUC2021 dataset consists of 15,683 DFU images and is categorized into four classes: control (normal DFU), infection only, ischemia only, and both infection and ischemia.

To evaluate the system's ability to distinguish between classes, the sigmoid oxygenation values derived from our system were averaged imagewise to produce a single biomarker for each image. A density histogram of oxygenation values for ulcers with ischemia vs ulcers without any issues was plotted in Figure 8 where a clear shift in the center of the distribution can be seen. We also plotted a density histogram for ulcers with infection vs ulcers with no issue in Figure 9, but no shift was present (which makes sense as infection doesn't necessarily affect the blood supply of the wound).

5 Discussion

5.1 Lighting

While MST++ and the rest of our system appear to be somewhat robust to various lighting conditions, as evidenced by our system producing a noticeable result in the case of the diabetic foot ulcer dataset, which was taken with several cameras under various indoor lighting conditions. The lack of lighting compensation or control still represents a major source of error for our system which we will be looking to address in future works, either by developing mobile attachments that provide even and spectrally neutral lighting or providing developments in lighting invariant spectral reconstruction techniques involving deep learning.

6 Conclusion

In this paper, we presented SigmoidOxy, a novel smartphone-based perfusion tool for the analysis of diabetic foot ulcer wounds. By leveraging modern spectral reconstruction, we demonstrated a high-performance method to extract insightful oxygenation information from standard RGB images captured by smartphone cameras. SigmoidOxy addresses a critical need in elderly care, where chronic wounds are challenging to manage. By providing an accurate, easy-to-use wound assessment app on the smartphone, our system empowers the elderly to monitor wound healing effectively at home.

References

[1] David G Armstrong, Mark A Swerdlow, Alexandria A Armstrong, Michael S Conte, William V Padula, and Sicco A Bus. 2020. Five year mortality and direct costs of care for people with diabetic foot complications are comparable to cancer. *Journal of foot and ankle research* 13 (2020), 1–4.

[2] Leonardo Ayala, Diana Mindroc-Filimon, Maike Rees, Marco Hübner, Jan Sellner, Silvia Seidlitz, Minu Tizabi, Sebastian Wirkert, Alexander Seitel, and Lena Maier-Hein. 2024. The SPECTRAL Perfusion Arm Clamping dAtaset (SPECTRALPACA) for video-rate functional imaging of the skin. *Scientific Data* 11, 1 (2024), 536.

[3] Yuanhao Cai, Jing Lin, Zudi Lin, Haoqian Wang, Yulun Zhang, Hanspeter Pfister, Radu Timofte, and Luc Van Gool. 2022. Mst++: Multi-stage spectral-wise transformer for efficient spectral reconstruction. In *Proceedings of the IEEE/CVF Conference on Computer Vision and Pattern Recognition.* 745–755.

[4] Neil T Clancy, Shobhit Arya, Danail Stoyanov, Mohan Singh, George B Hanna, and Daniel S Elson. 2015. Intraoperative measurement of bowel oxygen saturation using a multispectral imaging laparoscope. *Biomedical optics express* 6, 10 (2015), 4179–4190.

[5] Ying Fu, Yongrong Zheng, Lin Zhang, and Hua Huang. 2018. Spectral reflectance recovery from a single RGB image. *IEEE Transactions on Computational Imaging* 4, 3 (2018), 382–394.

[6] Qinghua He, Wanyu Li, Yaping Shi, Yi Yu, Wenqian Geng, Zhiyuan Sun, and Ruikang K Wang. 2023. SpeCamX: mobile app that turns unmodified smartphones into multispectral imagers. *Biomedical Optics Express* 14, 9 (2023), 4929–4946.

[7] Qinghua He and Ruikang Wang. 2020. Hyperspectral imaging enabled by an unmodified smartphone for analyzing skin morphological features and monitoring hemodynamics. *Biomedical optics express* 11, 2 (2020), 895–910.

[8] Longqian Huang, Ruichen Luo, Xu Liu, and Xiang Hao. 2022. Spectral imaging with deep learning. *Light: Science & Applications* 11, 1 (2022), 61.

[9] Berk Kaya, Yigit Baran Can, and Radu Timofte. 2019. Towards spectral estimation from a single RGB image in the wild. In *2019 IEEE/CVF International Conference on Computer Vision Workshop (ICCVW).* IEEE, 3546–3555.

[10] Alexander Kirillov, Eric Mintun, Nikhila Ravi, Hanzi Mao, Chloe Rolland, Laura Gustafson, Tete Xiao, Spencer Whitehead, Alexander C Berg, Wan-Yen Lo, et al. 2023. Segment anything. In *Proceedings of the IEEE/CVF International Conference on Computer Vision.* 4015–4026.

[11] Guolan Lu and Baowei Fei. 2014. Medical hyperspectral imaging: a review. *Journal of biomedical optics* 19, 1 (2014), 010901–010901.

[12] H Owen-Reece, M Smith, CE Elwell, and JC Goldstone. 1999. Near infrared spectroscopy. *British journal of anaesthesia* 82, 3 (1999), 418–426.

[13] Alberto J Pérez-Panero, María Ruiz-Muñoz, Antonio I Cuesta-Vargas, and Manuel Gónzalez-Sánchez. 2019. Prevention, assessment, diagnosis and management of diabetic foot based on clinical practice guidelines: A systematic review. *Medicine* 98, 35 (2019), e16877.

[14] Scott A Prahl. 1999. Tabulated molar extinction coefficient for hemoglobin in water. *http://omlc. ogi. edu/spectra/hemoglobin/summary. html* (1999).

[15] T Sarna and HA Swartz. 2006. The physical properties of melanin in The Pigmentary System. *Physiology and Pathophysiology (eds Nordlund, JJ et al.)* (2006), 311–341.

[16] Sebastian J Wirkert, Hannes Kenngott, Benjamin Mayer, Patrick Mietkowski, Martin Wagner, Peter Sauer, Neil T Clancy, Daniel S Elson, and Lena Maier-Hein. 2016. Robust near real-time estimation of physiological parameters from megapixel multispectral images with inverse Monte Carlo and random forest regression. *International journal of computer assisted radiology and surgery* 11 (2016), 909–917.

[17] Moi Hoon Yap, Bill Cassidy, Joseph M Pappachan, Claire O'Shea, David Gillespie, and Neil D Reeves. 2021. Analysis towards classification of infection and ischaemia of diabetic foot ulcers. In *2021 IEEE EMBS International Conference on Biomedical and Health Informatics (BHI)*. IEEE, 1–4.